WARWICK
THE UNIVERSITY OF WARWICK

Manuscript version: Published Version
The version presented in WRAP is the published version (Version of Record).

Persistent WRAP URL:
http://wrap.warwick.ac.uk/150236

How to cite:
The repository item page linked to above, will contain details on accessing citation guidance from the publisher.

Copyright and reuse:
The Warwick Research Archive Portal (WRAP) makes this work by researchers of the University of Warwick available open access under the following conditions.

Publisher's statement:
Please refer to the repository item page, publisher's statement section, for further information.

For more information, please contact the WRAP Team at: wrap@warwick.ac.uk

Pairing symmetry of an intermediate valence superconductor CeIr$_3$ investigated using μSR measurements

D. T. Adroja [1,2,*], A. Bhattacharyya [3,†], Y. J. Sato [4,5], M. R. Lees [6], P. K. Biswas [1], K. Panda [3], V. K. Anand,[7]
Gavin B. G. Stenning,[1] A. D. Hillier,[1] and D. Aoki[5]

[1]*ISIS Facility, Rutherford Appleton Laboratory, Chilton, Didcot Oxon OX11 0QX, United Kingdom*
[2]*Highly Correlated Matter Research Group, Department of Physics, University of Johannesburg,*
PO Box 524, Auckland Park 2006, South Africa
[3]*Department of Physics, Ramakrishna Mission Vivekananda Educational and Research Institute, Belur Math,*
Howrah 711202, West Bengal, India
[4]*Graduate School of Engineering, Tohoku University, Sendai 980-8577, Japan*
[5]*Institute for Materials Research, Tohoku University, Oarai, Ibaraki 311-1313, Japan*
[6]*Department of Physics, University of Warwick, Coventry CV4 7AL, United Kingdom*
[7]*Department of Physics, Indian Institute of Technology Delhi, Hauz Khas, New Delhi 110016, India*

We have investigated the bulk and microscopic properties of the rhombohedral intermediate valence superconductor CeIr$_3$ by employing magnetization, heat capacity, and muon spin rotation and relaxation (μSR) measurements. The magnetic susceptibility indicates bulk superconductivity below $T_C = 3.1$ K. Heat capacity data also reveal a bulk superconducting transition at 3.1 K with a second weak anomaly near 1.6 K. Zero-field μSR data show no strong evidence of broken time-reversal symmetry but support the presence of spin fluctuations below T_C. Transverse-field μSR measurements suggest a fully gapped, isotropic, s-wave superconductivity with $2\Delta(0)/k_B T_C = 3.76(3)$, very close to 3.53, the Bardeen-Cooper-Schrieffer gap value for weak-coupling superconductors. From the temperature variation of the magnetic penetration depth, we have also determined the London penetration depth $\lambda_L(0) = 435(2)$ nm, the carrier effective-mass enhancement $m^* = 1.69(1)m_e$, and the superconducting carrier density $n_s = 2.5(1) \times 10^{27}$ carriers m^{-3}. The fact that LaIr$_3$, with no $4f$ electrons, and CeIr$_3$ with $4f^n$ electrons where $n \leqslant 1$ (Ce ion in a valence fluctuating state), both exhibit the same s-wave gap symmetry indicates that the Ir-d band governs the physics of these two compounds near the Fermi level, which is in agreement with previous band structure calculations.

I. INTRODUCTION

The strongly correlated electron systems of Ce, Yb, and U have attracted considerable attention in condensed-matter physics, both theoretically and experimentally, due to the observation of heavy-fermion (HF) and valence fluctuation behavior, unconventional superconductivity, quantum criticality, and spin and charge gap formation [1]. The great interest in heavy-fermion systems originated with the identification of superconductivity in CeCu$_2$Si$_2$ with a $T_C = 0.7$ K [2]. At that time it was thought that magnetism and superconductivity would not occur simultaneously. Nevertheless, in CeCu$_2$Si$_2$ the $4f$ electrons which give rise to the local magnetic moments also seem to be responsible for the unconventional superconductivity [3]. Unconventional superconductivity was also reported in other Ce-based heavy-fermion compounds including CeCoIn$_5$, which has a T_C of 2.3 K [4,5], and the noncentrosymmetric HF superconductor CePt$_3$Si [6], a system without a center of inversion in the crystal structure that exhibits a coexistence of antiferromagnetic order

($T_N = 2.2$ K) and superconductivity ($T_C = 0.75$ K). Usually, the conventional Bardeen-Cooper-Schrieffer (BCS) theory of superconductivity does not apply to these exotic systems [7]. Heavy fermions have a diverse range of ground states, including superconductors such as UBe$_{13}$ [8] and UPt$_3$ [9,10], both with unconventional superconducting ground states. There are many magnetic HF systems which exhibit unconventional superconductivity under applied pressure. For example, CeIn$_3$ ($T_C = 0.2$ K at 2.46 GPa) [11], CePd$_2$Si$_2$ ($T_C = 0.43$ K at $\sim$3.0 GPa) [12], CeRh$_2$Si$_2$ ($T_C = 0.35$ K at 0.9 GPa) [13,14], and CeTX_3 (T = Co, Rh, Ir, X = Si and Ge; $T_C = 0.7$–1.3 K, 1–22 GPa) [15–24]. Many of these HF superconductors have high upper critical fields, and some of them exhibit anisotropic behavior. Furthermore, it is reported that the superconductivity in CeIn$_3$ and CeCoIn$_5$ has d-wave pairing symmetry, mainly induced by antiferromagnetic spin fluctuations, in a way that is very similar to the high-temperature cuprates [25,26]. Strong interest in heavy fermions is also generated by the similarities seen in the phase diagrams of HF superconductors and high-temperature superconductors, including the cuprates and Fe-based materials [27–30], where spin fluctuations are also suggested to play an important role.

Recently, RIr$_3$ (R = La and Ce) materials have attracted considerable attention both experimentally and theoretically

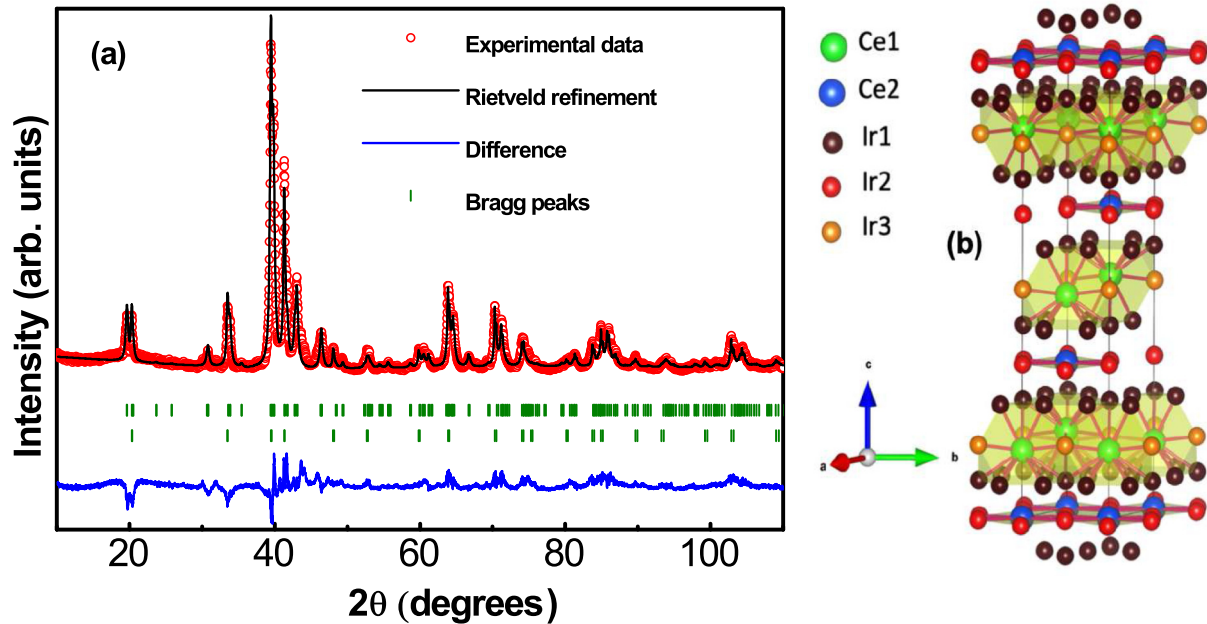*devashibhai.adroja@stfc.ac.uk
†amitava.bhattacharyya@rkmvu.ac.in

104514-1

FIG. 1. (a) Rietveld refinement of the powder x-ray diffraction pattern of CeIr$_3$. The data are shown as red circles and the result of the refinement as a solid line (black). We have used the rhombohedral phase (space group $R\bar{3}m$, No. 166) of CeIr$_3$ as the main phase and added CeIr$_2$ cubic phase (space group $Fd\bar{3}m$, No. 227) as an impurity phase. The vertical green bars show the Bragg peaks' positions, top for CeIr$_3$ phase and bottom for CeIr$_2$ phase. (b) Rhombohedral crystal structure of CeIr$_3$ where the Ce atoms are the bigger spheres, and the Ir atoms are the smaller spheres.

due to the observation of superconductivity with strong spin-orbit coupling [31–33]. CeIr$_3$ forms in a PuNi$_3$-type rhombohedral crystal structure (Fig. 1), space group $R\bar{3}m$ (166, D_{3d}^5) [32]. Sato *et al.* [32] reported bulk type-II superconductivity in CeIr$_3$ with $T_C = 3.4$ K, which is the second-highest T_C among the Ce-based intermetallic compounds. The crystal structure consists of two nonequivalent Ce sites (Ce1 and Ce2) and three Ir sites (Ir1, Ir2, and Ir3) [Fig. 1(b)]. Górnicka *et al.* [34] calculated the band structure of CeIr$_3$, which confirmed a nonmagnetic ground state, with a small contribution from the Ce 4f shell. It was reported that the density of states (DOS) at the Fermi surface principally arises from the 5d states of the Ir atoms, suggesting that CeIr$_3$ is indeed an Ir 5d-band superconductor and that the 5d electrons play a crucial role in the superconductivity. An x-ray photoelectron spectroscopy study reported that the Ce ions have a strong intermediate valence character in CeIr$_3$ [34]. The Ce ion valence of 3.6 in CeIr$_3$ was estimated using the superconducting transition temperatures, T_C, of the pseudobinaries of the isostructural compounds LaIr$_3$, CeIr$_3$, and ThIr$_3$ [35]. Furthermore, evidence of an intermediate valence, between 3$^+$ and 4$^+$, of the Ce ions in CeIr$_3$ comes from Vegard's law by plotting the volume versus covalent radius of the R^{3+} metal in the RIr$_3$ series. The volume increases monotonically with an increase in the radius, except for Ce, for which the unit-cell volume is much smaller and comparable with the unit-cell volume of GdIr$_3$ supporting the intermediate valence of Ce ion in CeIr$_3$ [34].

The isostructural compound LaIr$_3$, with $T_C = 2.5$ K, is another of the few materials [31–33] with 5d electrons that exhibits superconductivity. Here as well, the bands at the Fermi surface are dominated by the Ir 5d states with spin-orbit

coupling, without any contribution from the La orbitals; a similar situation is observed for CeRu$_2$ [35]. Very recently, we have investigated the superconducting properties of LaIr$_3$ using transverse-field (TF) and zero-field (ZF) muon spin rotation and relaxation (μSR) measurements. Our TF-μSR measurements revealed a fully gapped isotropic s-wave superconductivity with a gap to T_C ratio, $2\Delta(0)/k_B T_C = 3.31$, which is smaller than the value expected from the BCS theory of 3.53, implying weak-coupling superconductivity [33]. Moreover, zero-field μSR measurements showed that there are no spontaneous magnetic fields below T_C, which confirmed that the time-reversal symmetry is preserved in LaIr$_3$ [33].

Here we have investigated the superconducting state of intermediate valence CeIr$_3$ employing magnetization, heat capacity, and TF/ZF-μSR measurements. The temperature dependence of the magnetic penetration depth, determined by TF-μSR measurements, implies a fully gapped isotropic s-wave nature for the superconducting state. The ZF-μSR data show no strong evidence for spontaneous internal fields developing at or below T_C, and a weak temperature dependence in the ZF-μSR relaxation rate below 3 K is taken as evidence for the presence of spin fluctuations rather than the breaking of time-reversal symmetry.

II. EXPERIMENTAL DETAILS

A polycrystalline sample of CeIr$_3$ was prepared in a tetra arc furnace by arc melting stoichiometric quantities of the starting elements (Ce 99.9 wt%; Ir 99.999 wt%). The ingot was flipped and remelted five times, and the sample was quenched. The sample was subsequently annealed at 900 °C

for 6 days under a vacuum of 1×10^{-4} Pa in a quartz ampoule. The sample was wrapped in tantalum foil during the annealing. The sample was heated to $900\,^\circ$C and held at this temperature for 6 days and then quenched by switching off the furnace. The quality of the sample was verified through powder x-ray diffraction using a Panalytical X-Pert Pro diffractometer. The temperature and field dependence of magnetization was measured using a Quantum Design Magnetic Property Measurement System SQUID magnetometer. Heat capacity down to 500 mK was measured using a Quantum Design Physical Property Measurement System with a ^{3}He insert. To examine the superconducting pairing symmetry and microscopic superconducting properties of CeIr$_3$, we performed TF/ZF μSR experiments at the muon beamline of the ISIS Pulsed Neutron and Muon Facility at the Rutherford Appleton Laboratory, United Kingdom, using the MUSR spectrometer [36]. The powder sample of CeIr$_3$ was mounted on a silver plate (99.995%) using GE varnish diluted with ethanol and covered with a silver foil. The sample was cooled to 50 mK using a dilution refrigerator. 100% spin-polarized positive muons were implanted into the sample, and the asymmetry of the resulting decay positrons was estimated using $P_z(t) = [N_F(t) - cN_B(t)]/[N_F(t) + cN_B(t)]$, where $N_B(t)$ and $N_F(t)$ are the number of positrons counted in the backward and forward detectors, respectively, and c is an instrumental calibration constant determined in the normal state with a small (2 mT) transverse magnetic field. The TF-μSR data were collected at different temperatures between 0.05 and 4 K in the presence of a 40-mT ($> \mu_0 H_{c1}(0) = 5.1(2)\,$mT) magnetic field. ZF data were collected between 0.05 and 4 K. To reduce the impact of any magnetic fields at the sample position in the ZF data, correction coils were used which assured the stray fields were always less than $1\,\mu$T. All the μSR data were analyzed using WIMDA, a muon data analysis program [37].

III. RESULTS AND DISCUSSION

A. Crystal structure and physical properties

Figure 1(a) presents the powder x-ray diffraction (XRD) pattern and a Rietveld refinement of the data for our polycrystalline sample of CeIr$_3$. CeIr$_3$ crystallizes in the PuNi$_3$-type rhombohedral structure with the space group $R\bar{3}m$, No. 166. Analysis of the XRD data reveals the fit can be improved by adding a small quantity of cubic CeIr$_2$ (space group $Fd\bar{3}m$, No. 227) as an impurity phase, although an overlap of the peaks for the two structures prevents a quantitative analysis. A schematic of the unit cell obtained from the Rietveld analysis of the XRD data of CeIr$_3$ is shown in the inset of Fig. 1(b). The lattice parameters of the synthesized CeIr$_3$ sample are $a = 5.2943(2)\,$Å and $c = 26.2134(1)\,$Å, which are in agreement with a previous report [32]. Electron probe microanalysis (EPMA) shows that the composition of the polycrystalline sample is 26(1) Ce: 74(1) Ir, which is close to the expected stoichiometry of the CeIr$_3$ phase, and there is no evidence for the presence of CeIr$_2$ (see Supplemental Material [38] for more details).

Figure 2(a) presents the temperature dependence of the magnetic susceptibility $\chi(T)$ in the zero-field-cooled (ZFC) and field-cooled-cooling (FCC) states, which confirms the bulk type-II superconductivity at 3.1 K in CeIr$_3$. The isothermal magnetic field dependence of the magnetization at 0.4 K is shown in Fig. 2(b). Figure 2(c) shows the temperature dependence of the heat capacity C_P at different applied magnetic fields. The inset in Fig. 2(c) shows the temperature variation of heat capacity at zero applied magnetic field. A clear signature of a superconducting transition is observed at 3.1 K in the $C_P(T)$ data. Another weaker transition in $C_P(T)$ is seen below 1.6 K. The heat capacity of single-crystal CeIr$_3$ shows only one transition at $T_C = 3.1$ K, as shown in Fig. 2(d), with no sign of a second transition [32]. This suggests that the second transition observed in the polycrystalline CeIr$_3$ near 1.6 K might be related to a superconducting impurity phase or a small variation in either the Ce or Ir content [31,34]. It is to be noted that LaIr$_3$ has a $T_C = 3.3$ K, while LaIr$_{2.8}$ has a $T_C = 2.75$ K [31]. Sugawara et al. [39] reported superconductivity in CeIr$_2$ at 0.25 K. In order to confirm that the transition near 1.6 K does not arise from CeIr$_2$, we have synthesized a polycrystalline sample of CeIr$_2$ and carried out a powder XRD study and measured the temperature dependence of the heat capacity, $C_P(T)$, of this sample down to 400 mK. The results are given in the Supplemental Material [38] and confirm that the weak anomaly observed in the heat capacity data of CeIr$_3$ near 1.6 K is not due to CeIr$_2$. We also considered the possibility that the anomaly is due to superconducting CeIr$_5$, which has a reported T_C of 1.8–1.9 K [38,40]. However, there is no evidence for CeIr$_5$ in the XRD or magnetic susceptibility data of our polycrystalline CeIr$_3$ sample. The anomaly at 1.6 K, therefore, requires further investigation. The jump in the heat capacity of CeIr$_3$ is suppressed in a magnetic field of 6 T. The heat capacity data were fitted using $C_P(T)/T = \gamma + \beta T^2$, where γ and β are the electronic Sommerfeld coefficient and lattice specific heat coefficient, respectively. The least-squares fit yields $\gamma = 21.66(2)\,$mJ/(mol K^2), $\beta = 1.812(1)\,$mJ/(mol K^4), and then using $\beta = n\frac{12}{5}\pi^4 R\Theta_D^{-3}$, where R is the universal gas constant and n is the number of atoms per formula unit, we estimate that the Debye temperature $\Theta_D = 162(2)\,$K, which is similar to the Θ_D values of isostructural ThIr$_3$ (169 K) [41] and DyIr$_3$ (155 K) [42]. For comparison, in Fig. 2(d) we have also plotted the heat capacity of single-crystal CeIr$_3$ reported by Sato et al. [32]. The jump in the heat capacity $\Delta C_e/\gamma T_C \sim 1.39(1)$ and the ratio $2\Delta(0)/k_B T_C = 3.83(1)$ both suggest that CeIr$_3$ can be categorized as a weak-coupling superconductor.

The inset in Fig. 2(a) shows the temperature dependence of the magnetic susceptibility measured in a magnetic field of 0.5 T for both CeIr$_3$ and LaIr$_3$. The susceptibility of CeIr$_3$ is higher than that of LaIr$_3$ and exhibits considerable temperature dependence below 25 K. This low-temperature rise could be attributed to a Curie tail from impurities [34]. At high temperatures (50–300 K) the weak temperature dependence of the susceptibility of CeIr$_3$ indicates the presence of strong hybridization between localized 4f electrons and conduction electrons, and the intermediate valence of the Ce ions.

B. Superconducting gap structures

The TF-μSR asymmetry spectra measured in an applied magnetic field of 40 mT are displayed in Figs. 3(a) and 3(b). The data in Fig. 3(a) were taken at the base temperature in the
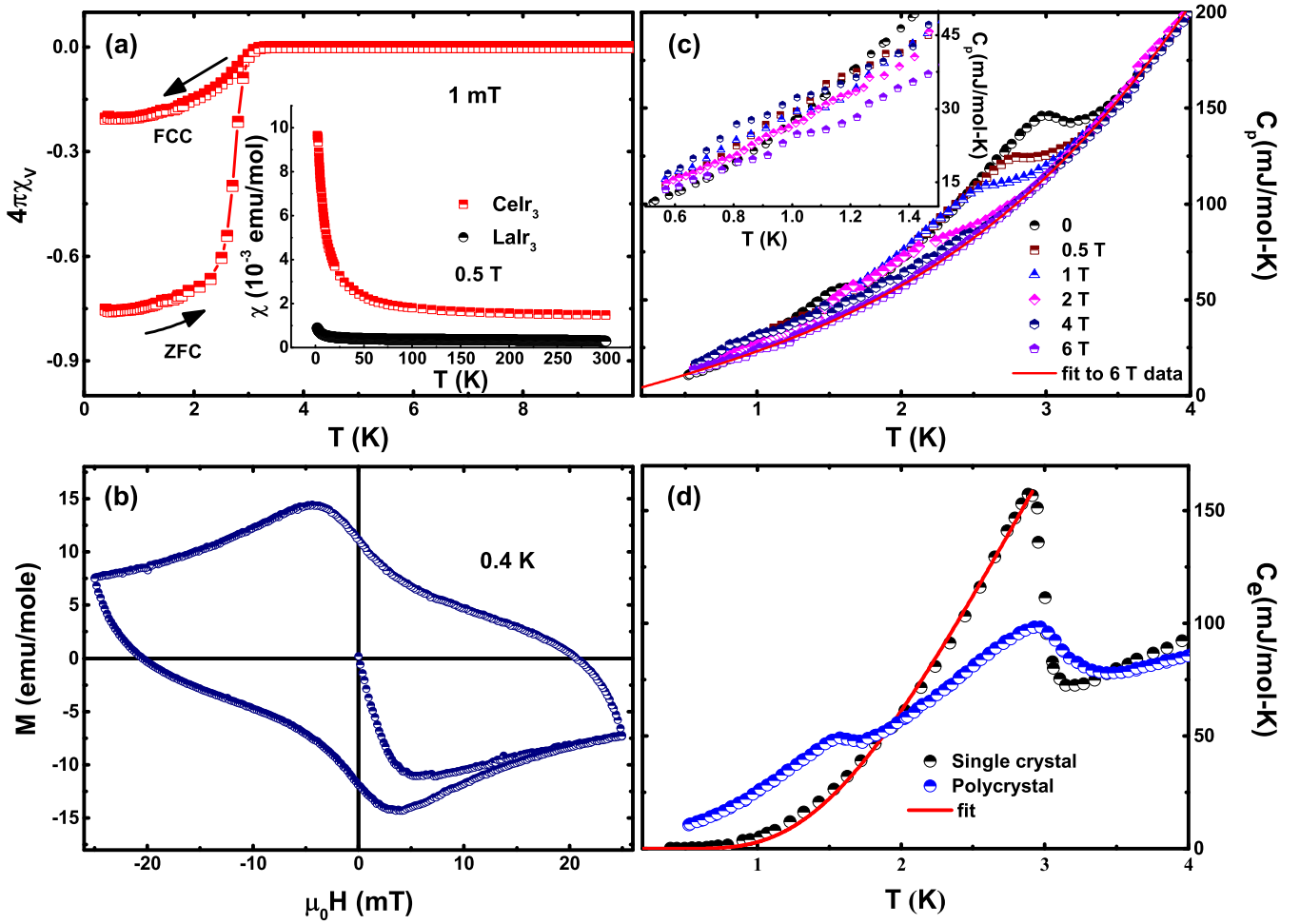
FIG. 2. (a) Temperature dependence of the dc magnetic susceptibility of CeIr$_3$ in zero-field-cooled (ZFC) and field-cooled-cooling (FCC) mode. The inset shows the temperature dependence of the magnetic susceptibility of CeIr$_3$ (red squares) and LaIr$_3$ (black circles) measured in a field of 0.5 T. (b) Isothermal magnetic field dependence of the magnetization of CeIr$_3$ at 0.4 K. (c) Temperature dependence of the heat capacity of CeIr$_3$ at different applied fields. The solid line shows a fit to the 6-T data. The inset shows the low-temperature heat capacity versus temperature in various applied magnetic fields on an expanded scale. (d) Electronic heat capacity for CeIr$_3$ single crystal from Ref. [32] presented here for comparison with the data for polycrystalline CeIr$_3$. The solid red line represents a fit to fully gapped superconductivity [32].

superconducting state and in Fig. 3(b) at a higher temperature, well into the normal state. At $T \geqslant T_C$, the muon asymmetry oscillates with minimal damping, suggesting that the internal field distribution is extremely uniform. On the other hand, the asymmetry spectrum measured at $T \leqslant T_C$ shows an increase in damping, suggesting an inhomogeneous field distribution due to the vortex state. To obtain quantitative information about the superconducting state in CeIr$_3$, we first tried to analyze the TF-μSR data recorded at various temperatures using two Gaussian components, one to account for the CeIr$_3$ phase and another to account for any impurity phase. However, the two-component model gave unphysical values for the parameters, and the fit did not converge. We therefore fitted our TF-μSR data using a single Gaussian model [43–46] given by

$$G_x(t) = C_1 \cos(\omega_1 t + \Phi) \exp\left(\frac{-\sigma^2 t^2}{2}\right)$$
$$+ C_2 \cos(\omega_2 t + \Phi), \qquad (1)$$

where C_i and ω_i ($i = 1, 2$) are the transverse-field asymmetries and the muon spin precision frequencies that arise from the sample and the silver sample holder (this could also include any impurity phase), and Φ and σ are a phase factor and total Gaussian depolarization rate, respectively. During the fitting C_2 was fixed at 35%, its low-temperature value, and the asymmetry spectra were then fit by varying the value of C_1, which is nearly independent of temperature. The phase, Φ, was also fixed to the value obtained at low temperatures. Figures 3(a) and 3(b) also include fits to the data (the solid red lines) using Eq. (1) and show a good correspondence between the experimental and the calculated asymmetry spectra.

The values of σ determined from the fits consist of two parts: one part comes from the superconducting signal σ_{sc} and the other part is the nuclear magnetic dipolar contribution σ_{nm}, which is taken to be constant over the entire temperature range studied. The superconducting depolarization rate σ_{sc} is then calculated using $\sigma_{sc} = \sqrt{\sigma^2 - \sigma_{nm}^2}$. The temperature variation of σ_{sc} is shown in Fig. 3(c). It is to be noted that there is no clear feature in the σ_{sc} data at 1.6 K [Fig. 3(c)], where the heat
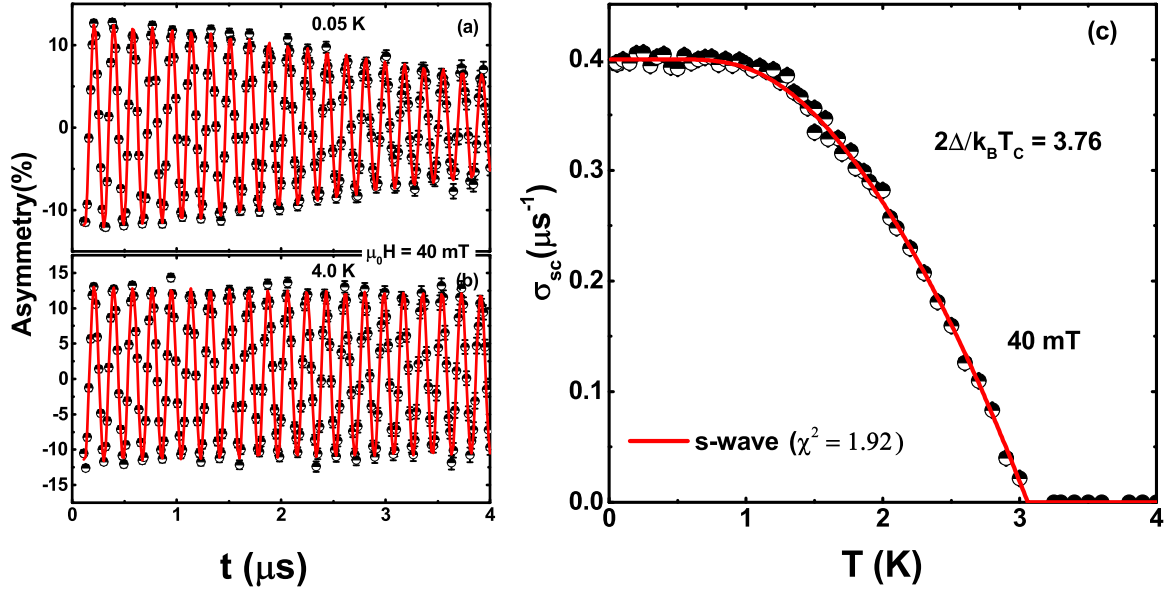
FIG. 3. TF-μSR spin precession signals for CeIr$_3$ collected in a transverse magnetic field of $\mu_0 H = 40$ mT. Asymmetry vs time in (a) the superconducting state at 0.05 K and (b) the normal state at 4.0 K. Solid lines represent fits to the data using Eq. (1). (c) Temperature variation of the Gaussian superconducting relaxation rate $\sigma_{sc}(T)$. The solid line is a fit to the data using an isotropic, fully gapped s-wave model using Eq. (2).

capacity exhibits a second anomaly. The σ_{sc} is modeled using a standard expression within the local London approximation [43,45,47] with

$$\frac{\sigma_{sc}(T)}{\sigma_{sc}(0)} = \frac{\lambda^{-2}(T, \Delta_0)}{\lambda^{-2}(0, \Delta_0)}$$
$$= 1 + 2 \int_{\Delta(T)}^{\infty} \left(\frac{\delta f}{\delta E} \right) \frac{E dE}{\sqrt{E^2 - \Delta^2(T)}}, \quad (2)$$

where $f = [1 + \exp(-E/k_B T)]^{-1}$ is the Fermi function and $\Delta(T, 0) = \Delta_0 \delta(T/T_C)$. Δ_0, the gap value at zero temperature, is the only adjustable parameter. The temperature dependence of the gap can be approximated by $\delta(T/T_C) =$ tanh $[1.82[1.018(T_C/T - 1)]^{0.51}]$ [48–50]. A conventional isotropically gapped model describes the data very well, as shown by the solid red line in Fig. 3(c). Using this isotropic model the refined critical temperature is $T_C = 3.1$ K, and the gap to T_C ratio of $2\Delta(0)/k_B T_C = 3.76(3)$ is close to the value of 3.53 expected from a weak-coupling BCS theory. This value is in agreement with the heat capacity data for single-crystal CeIr$_3$.

Using the TF-μSR results, the other superconducting parameters characterizing the superconducting ground state of CeIr$_3$ can be evaluated. For a triangular lattice $\frac{\sigma_{sc}^2(T)}{\gamma_\mu^2} = 0.00371 \frac{\phi_0^2}{\lambda^4}$, where ϕ_0 is the flux quantum number 2.07×10^{-15} T m^2 and γ_μ is the muon gyromagnetic ratio, $\gamma_\mu/2\pi = 135.5$ MHz T^{-1}. Using this relation we have estimated the magnetic penetration depth, $\lambda(0) = 435(2)$ nm. The London theory [51] gives the relation between microscopic quantities λ (or λ_L), effective mass m^*, and the superconducting carrier density n_s, $\lambda_L^2 = \lambda^2 = \frac{m^* c^2}{4\pi n_s e^2}$, here $m^* = (1 + \lambda_{e-ph}) m_e$, where λ_{e-ph} is the electron-phonon coupling constant and m_e is an electron mass. Using McMillan's relation [52], λ_{e-ph} can

be determined using

$$\lambda_{e-ph} = \frac{1.04 + \mu^* \ln(\Theta_D/1.45 T_C)}{(1 - 0.62\mu^*) \ln(\Theta_D/1.45 T_C) - 1.04}, \quad (3)$$

where Θ_D is the Debye temperature. Assuming a repulsive screened Coulomb parameter $\mu^* = 0.13$ [53], we have estimated $\lambda_{e-ph} = 0.57(2)$. This value of λ_{e-ph} is larger than 0.02–0.2 observed for many Fe-based superconductors (11 and 122 families) and cuprates (YBCO-123) [54] but smaller than 1.38 for LiFeAs [55], 1.53 for PrFeAsO$_{0.60}$F$_{0.12}$ [56], and 1.2 for LaO$_{0.9}$F$_{0.1}$FeAs [57]. Given CeIr$_3$ is a type-II superconductor, using the value of λ_{e-ph} estimated above and λ_L, we find the effective-mass enhancement $m^* = 1.69(1)m_e$ and superconducting carrier density $n_s = 2.5(1) \times 10^{27}$ carriers m^{-3}. The superconducting parameters of CeIr$_3$ and LaIr$_3$ are listed together in Table I.

TABLE I. Superconducting parameters of CeIr$_3$ and LaIr$_3$. The parameter values of LaIr$_3$ come from Ref. [33].

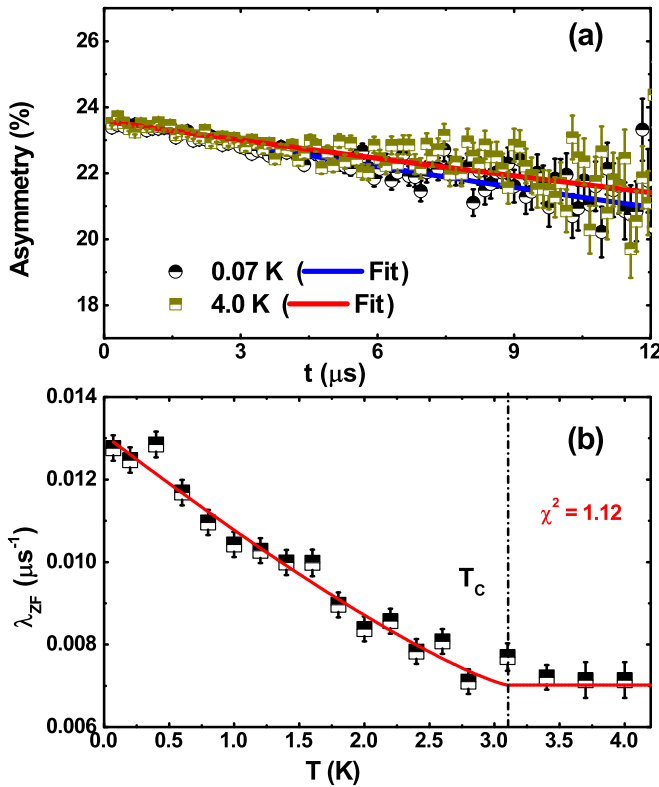| Parameter (units)	CeIr$_3$	LaIr$_3$
T_C (K)	3.1	2.5
$\mu_0 H_{c1}$ (mT)	5.1(2)	11.0(2)
$\mu_0 H_{c2}$ (T)	4.65(3)	1.52(1)
$\gamma(0)$ (mJ/mol K^2)	21.66(2)	15.32(3)
Θ_D (K)	162(2)	430(4)
$\Delta C/\gamma T_C$	1.39(1)	1.0(2)
$2\Delta/k_B T_C$	3.76(3)	3.31(1)
λ (nm)	435(2)	386(3)
λ_{e-ph}	0.57(2)	0.53(3)
n_s ($\times 10^{27}$ carriers/m^3)	2.5(1)	2.9(1)

FIG. 4. (a) Zero-field μSR asymmetry spectra for CeIr$_3$ collected at 0.07 K (black circles) and 4.0 K (dark yellow squares) together with solid lines that are least-squares fits to the data using Eq. (4). (b) Temperature dependence of the zero-field muon relaxation rate. The solid red line indicates a fit made to a power-law behavior using $\lambda_{ZF}(T) = \lambda_{ZF}(0)[1 - (T/T_C)^\alpha]^\beta + a_1$ with T_C fixed at 3.1 K (see text).

C. Zero-field muon spin relaxation

ZF-μSR muon asymmetry spectra above (dark yellow) and below (black) T_C that are representative of the data collected are shown in Fig. 4(a). Both spectra exhibit a slow and almost indistinguishable exponential relaxation. Fits to the ZF-μSR spectra at several temperatures between 0.07 and 4.0 K were made using the Lorentzian function as used for other superconductors [45,58–61],

$$G_z(t) = A_0 \exp(-\lambda_{ZF}t) + A_{bg}, \qquad (4)$$

where A_0, A_{bg}, and λ_{ZF} are the total initial asymmetry from muons probing the sample, the asymmetry arising from muons landing in the silver sample holder, and the electronic relaxation rate, respectively. The parameters A_0 and A_{bg} are found to be temperature independent. The zero-field-μSR measurements reveal that the relaxation rate between 0.07 and 4 K is only slightly temperature dependent [see Fig. 4(b)], with a weak inflexion as the temperature is reduced below $T_C = 3.1$ K.

If the temperature dependence of the ZF relaxation rate was due to extrinsic impurities, the relaxation ought to saturate below some temperature, independently of T_C, or go through a maximum and then decrease. The absence of this behavior indicates that the temperature dependence of the ZF relaxation is an intrinsic property of the CeIr$_3$ phase.

We have fitted the ZF relaxation rate using a phenomenological power law, $\lambda_{ZF}(T) = \lambda_{ZF}(0)[1 - (T/T_C)^\alpha]^\beta + a_1$, where a_1 is the temperature-independent relaxation rate above T_C. We have fixed α at 1 and T_C at 3.1 K. The values of the parameters obtained are $\beta = 1.23(9)$, $\lambda_{ZF}(0) = 0.0061(2) \, \mu s^{-1}$, and $a_1 = 0.0071(1) \, \mu s^{-1}$. The fit is shown by a solid line in Fig. 4(b). It is to be noted that when we allowed α to vary its value remained close to 1. A similar analysis was performed for the ZF-μSR relaxation rate in UPt$_3$ [62], and the reported values for the parameters are (sample dependent) $\alpha = 0.89 - 1$ and $\beta = 1.53 - 2.1$. For UPt$_3$, the ZF relaxation rate saturates at the lowest temperature and the observed temperature dependence was attributed to broken time-reversal symmetry. In CeIr$_3$ the relaxation rate increases almost linearly down to the lowest temperature, and there is no obvious mechanism to break time-reversal symmetry in this s-wave centrosymmetric material. Without further work, we conclude that time-reversal symmetry is likely preserved in CeIr$_3$.

Instead, we suggest this relaxation, which may be slightly enhanced below T_C, is due to the presence of weak spin fluctuations. This effect is not seen in LaIr$_3$, which suggests that the spin fluctuations originate from the Ce moments that are in an intermediate valence state. Similar changes in $\lambda_{ZF}(T)$ have been observed in other superconducting materials, for example, in the cuprate superconductor YBa$_2$Cu$_3$O$_y$, which exhibits a change in $\lambda_{ZF}(T)$ below the pseudogap temperature due to slowly fluctuating magnetic fields [63]. Changes in ZF relaxation rate around T_C observed in the pnictide superconductor SmFeAsO$_{1-x}$F$_x$ [64], the rare-earth based superconductors RRuB$_2$ where $R =$ Lu or Y [65], and the quasi-one-dimensional superconductor Cs$_2$Cr$_3$As$_3$ [59] have all been attributed to spin fluctuations.

IV. SUMMARY

In summary, we have examined the superconducting properties, including the superconducting ground state, of CeIr$_3$. Magnetic susceptibility measurements show that CeIr$_3$ is a bulk type-II superconductor with $T_C = 3.1$ K. The heat capacity of polycrystalline CeIr$_3$ shows the superconducting transition near 3.1 K and a second, weaker anomaly near 1.6 K. Given that the heat capacity of CeIr$_3$ single crystal exhibits only one transition near $T_C = 3.1$ K [31] and no peak is observed in the heat capacity of CeIr$_2$ between 400 mK and 2.5 K [38], the second transition near 1.6 K could be associated with some variation in Ce/Ir content throughout the polycrystalline sample, and this issue requires further investigation. The temperature dependence of the ZF-μSR relaxation rate suggests the presence of weak spin fluctuations in CeIr$_3$. Transverse-field μSR measurements reveal that CeIr$_3$ exhibits an isotropic fully gapped s-wave-type superconductivity with a gap to T_C ratio, $2\Delta(0)/k_B T_C = 3.76$, compared to the expected BCS value of 3.53, suggesting weak-coupling superconductivity. The s-wave pairing symmetry observed in both LaIr$_3$ [33], a material with no $4f$ electrons, and CeIr$_3$, with less than one $4f$ electron, indicates that the superconductivity is controlled by the Ir-d bands near the Fermi level in both compounds.

ACKNOWLEDGMENTS

[1] P. Coleman, *Introduction to Many-Body Physics* (Cambridge University Press, Cambridge, 2015).

[2] F. Steglich, J. Aarts, C. D. Bredl, W. Lieke, D. Meschede, W. Franz, and H. Schäfer, Phys. Rev. Lett. **43**, 1892 (1979).

[3] M. Smidman, O. Stockert, J. Arndt, G. M. Pang, L. Jiao, H. Q. Yuan, H. A. Vieyra, S. Kitagawa, K. Ishida, K. Fujiwara, T. C. Kobayashi, E. Schuberth, M. Tippmann, L. Steinke, S. Lausberg, A. Steppke, M. Brando, H. Pfau, U. Stockert, P. Sun *et al.*, Philos. Mag. **98**, 2930 (2018).

[4] C. Petrovic, P. G. Pagliuso, M. F. Hundley, R. Movshovich, J. L. Sarrao, J. D. Thompson, Z. Fisk, and P. Monthoux, J. Phys.: Condens. Matter **13**, L337 (2001).

[5] V. A. Sidorov, M. Nicklas, P. G. Pagliuso, J. L. Sarrao, Y. Bang, A. V. Balatsky, and J. D. Thompson, Phys. Rev. Lett. **89**, 157004 (2002).

[6] E. Bauer, G. Hilscher, H. Michor, Ch. Paul, E. W. Scheidt, A. Gribanov, Yu. Seropegin, H. Noël, M. Sigrist, and P. Rogl, Phys. Rev. Lett. **92**, 027003 (2004).

[7] J. Bardeen, L. N. Cooper, and J. R. Schrieffer, Phys. Rev. **106**, 162 (1957).

[8] M. W. McElfresh, J. H. Hall, R. R. Ryan, J. L. Smith, and Z. Fisk, Acta Cryst. **C46**, 1579 (1990).

[9] A. de Visser, J. J. M. Franse, and A. Menovsky, J. Magn. Magn. Mater. **43**, 43 (1984).

[10] T. Trappmann and H. v. Löhneysen, and L. Taillefer, Phys. Rev. B **43**, 13714 (1991).

[11] G. Knebel, D. Braithwaite, P. C. Canfield, G. Lapertot, and J. Flouquet, Phys. Rev. B **65**, 024425 (2001).

[12] N. D. Mathur, F. M. Grosche, S. R. Julian, I. R. Walker, D. M. Freye, R. K. W. Haselwimmer, and G. G. Lonzarich, Nature (London) **394**, 39 (1998).

[13] R. Movshovich, T. Graf, D. Mandrus, J. D. Thompson, J. L. Smith, and Z. Fisk, Phys. Rev. B **53**, 8241 (1996).

[14] S. Araki, M. Nakashima, R. Settai, T. C. Kobayashi, and Y. Ōnuki, J. Phys.: Condens. Matter **14**, L377 (2002).

[15] Y. Muro, D. Eom, N. Takeda, and M. Ishikawa, J. Phys. Soc. Jpn. **67**, 3601 (1998).

[16] N. Kimura, K. Ito, K. Saitoh, Y. Umeda, H. Aoki, and T. Terashima, Phys. Rev. Lett. **95**, 247004 (2005).

[17] N. Kimura, Y. Muro, and H. Aoki, J. Phys. Soc. Jpn. **76**, 051010 (2007).

[18] I. Sugitani, Y. Okuda, H. Shishido, T. Yamada, A. Thamizhavel, E. Yamamoto, T. D. Matsuda, Y. Haga, T. Takeuchi, R. Settai, and Y. Ōnuki, J. Phys. Soc. Jpn. **75**, 043703 (2006).

[19] Y. Okuda, Y. Miyauchi, Y. Ida, Y. Takeda, C. Tonohiro, Y. Oduchi, T. Yamada, N. D. Dung, T. D. Matsuda, Y. Haga, T. Takeuchi, M. Hagiwara, K. Kindo, H. Harima, K. Sugiyama, R. Settai, and Y. Ōnuki, J. Phys. Soc. Jpn. **76**, 044708 (2007).

[20] R. Settai, I. Sugitani, Y. Okuda, A. Thamizhavel, M. Nakashima, Y. Ōnuki, and H. Harima, J. Magn. Magn. Mater. **310**, 844 (2007).

[21] G. Knebel, D. Aoki, G. Lapertot, B. Salce, J. Flouquet, T. Kawai, H. Muranaka, R. Settai, and Y. Ōnuki, J. Phys. Soc. Jpn. **78**, 074714 (2009).

[22] A. Thamizhavel, T. Takeuchi, T. D. Matsuda, Y. Haga, K. Sugiyama, R. Settai, and Y. Ōnuki, J. Phys. Soc. Jpn. **74**, 1858 (2005).

[23] T. Kawai, H. Muranaka, M.-A. Measson, T. Shimoda, Y. Doi, T. Matsuda, Y. Haga, G. Knebel, G. Lapertot, D. Aoki, J. Flouquet, T. Takeuchi, R. Settai, and Y. Ōnuki, J. Phys. Soc. Jpn. **77**, 064716 (2008).

[24] F. Honda, I. Bonalde, K. Shimizu, S. Yoshiuchi, Y. Hirose, T. Nakamura, R. Settai, and Y. Ōnuki, Phys. Rev. B **81**, 140507(R) (2010).

[25] H. Fukazawa and K. Yamada, J. Phys. Soc. Jpn. **72**, 2449 (2003).

[26] C. Stock, C. Broholm, J. Hudis, H. J. Kang, and C. Petrovic, Phys. Rev. Lett. **100**, 087001 (2008).

[27] A. Grauel, A. Böhm, H. Fischer, C. Geibel, R. Köhler, R. Modler, C. Schank, F. Steglich, G. Weber, T. Komatsubara, and N. Sato, Phys. Rev. B **46**, 5818(R) (1992).

[28] Q. Si and F. Steglich, Science **329**, 1161 (2010).

[29] J. Zhao, Q. Huang, C. de la Cruz, S. Li, J. W. Lynn, Y. Chen, M. A. Green, G. F. Chen, G. Li, Z. Li, J. L. Luo, N. L. Wang, and P. Dai, Nat. Mater. **7**, 953 (2008).

[30] J. Paglione and R. L. Greene, Nat. Phys. **6**, 645 (2010).

[31] N. Haldolaarachchige, L. Schoop, M. A. Khan, W. Huang, H. Ji, K. Hettiarachchilage, and D. P. Young, J. Phys.: Condens. Matter **29**, 475602 (2017).

[32] Y. J. Sato, A. Nakamura, Y. Shimizu, A. Maurya, Y. Homma, D. Li, F. Honda, and D. Aoki, J. Phys. Soc. Jpn. **87**, 053704 (2018); Y. J. Sato, F. Honda, Y. Shimizu, A. Nakamura, Y. Homma, A. Maurya, D. Li, T. Koizumi, and D. Aoki, Phys. Rev. B **102**, 174503 (2020).

[33] A. Bhattacharyya, D. T. Adroja, P. K. Biswas, Y. J. Sato, M. R. Lees, D. Aoki, and A. D. Hillier, J. Phys.: Condens. Matter **32**, 065602 (2020).

[34] K. Górnicka, E. M. Carnicom, S. Gołąb, M. Łapiński, B. Wiendlocha, W. Xie, D. Kaczorowski, R. J. Cava, and T. Klimczuk, Supercond. Sci. Technol. **32**, 025008 (2019).

[35] M. Hakimi and J. G. Huber, Physica B+C **135**, 434 (1985).

[36] S. L. Lee, S. H. Kilcoyne, and R. Cywinski, *Muon Science: Muons in Physics, Chemistry, and Materials* (SUSSP Publications and IOP Publishing, Bristol, 1999).

[37] F. L. Pratt, Physica B **289-290**, 710 (2000).

[38] See Supplemental Material at http://link.aps.org/supplemental/10.1103/PhysRevB.103.104514 for electron probe microanalysis of the polycrystalline sample of $CeIr_3$ and powder x-ray

diffraction and heat capacity measurements on polycrystalline $CeIr_2$.

[39] H. Sugawara, T. Yamazaki, J. Itoh, M. Takashita, T. Ebihara, N. Kimura, P. Svoboda, R. Settai, Y. Onuki, H. Sato, S. Uji, and H. Aoki, J. Phys. Soc. Jpn. **63**, 1502 (1994).

[40] J. Tang, Ph.D. thesis, Iowa State University, 1989.

[41] K. Górnicka, D. Das, S. Gutowska, B. Wiendlocha, M. J. Winiarski, T. Klimczuk, and D. Kaczorowski, Phys. Rev. B **100**, 214514 (2019).

[42] B. Mondal, S. Dan, S. Mondal, R. N. Bhowmik, R. Ranganathan, and C. Mazumdar, Intermetallics **120**, 106740 (2020).

[43] A. Bhattacharyya, D. T. Adroja, J. Quintanilla, A. D. Hillier, N. Kase, A. M. Strydom, and J. Akimitsu, Phys. Rev. B **91**, 060503(R) (2015).

[44] A. Bhattacharyya, D. T. Adroja, N. Kase, A. D. Hillier, J. Akimitsu, and A. M. Strydom, Sci. Rep. **5**, 12926 (2015).

[45] D. T. Adroja, A. Bhattacharyya, M. Telling, Yu. Feng, M. Smidman, B. Pan, J. Zhao, A. D. Hillier, F. L. Pratt, and A. M. Strydom, Phys. Rev. B **92**, 134505 (2015).

[46] A. Bhattacharyya, D. T. Adroja, M. Smidman, and V. K. Anand, Sci. China-Phys. Mech. Astron. **61**, 127402 (2018).

[47] A. Bhattacharyya, D. T. Adroja, K. Panda, S. Saha, T. Das, A. J. S. Machado, O. V. Cigarroa, T. W. Grant, Z. Fisk, A. D. Hillier, and P. Manfrinetti, Phys. Rev. Lett. **122**, 147001 (2019).

[48] R. Prozorov and R. W. Giannetta, Supercond. Sci. Technol. **19**, R41 (2006).

[49] J. F. Annett, Adv. Phys. **39**, 83 (1990).

[50] G. M. Pang, M. Smidman, W. B. Jiang, J. K. Bao, Z. F. Weng, Y. F. Wang, L. Jiao, J. L. Zhang, G. H. Cao, and H. Q. Yuan, Phys. Rev. B **91**, 220502(R) (2015).

[51] J. E. Sonier, J. H. Brewer, and R. F. Kiefl, Rev. Mod. Phys. **72**, 769 (2000).

[52] W. L. McMillan, Phys. Rev. **167**, 331 (1968).

[53] P. B. Allen, in *Handbook of Superconductivity*, edited by C. P. Poole, Jr. (Academic Press, New York, 1999), Chap. 9, p. 478.

[54] A.-M. Zhang and Q.-M. Zhang, Chin. Phys. B **22**, 087103 (2013).

[55] A. A. Kordyuk, V. B. Zabolotnyy, D. V. Evtushinsky, T. K. Kim, I. V. Morozov, M. L. Kulić, R. Follath, G. Behr, B. Büchner, and S. V. Borisenko, Phys. Rev. B **83**, 134513 (2011).

[56] D. Bhoi, P. Mandal, and P. Choudhury, Supercond. Sci. Technol. **21**, 125021 (2008).

[57] G. Mu, X.-Y. Zhu, L. Fang, L. Shan, C. Ren, and H.-H. Wen, Chin. Phys. Lett. **25**, 2221 (2008).

[58] D. T. Adroja, A. Bhattacharyya, P. K. Biswas, M. Smidman, A. D. Hillier, H. Mao, H. Luo, G.-H. Cao, Z. Wang, and C. Wang, Phys. Rev. B **96**, 144502 (2017).

[59] D. Adroja, A. Bhattacharyya, M. Smidman, A. Hillier, Yu. Feng, B. Pan, J. Zhao, M. R. Lees, A. Strydom, and P. K. Biswas, J. Phys. Soc. Jpn. **86**, 044710 (2017).

[60] A. Bhattacharyya, D. T. Adroja, A. D. Hillier, R. Jha, V. P. S. Awana, and A. M. Strydom, J. Phys.: Condens. Matter **29**, 265602 (2017).

[61] A. Bhattacharyya, K. Panda, D. T. Adroja, N. Kase, P. K. Biswas, S. Saha, T. Das, M. R. Lees, and A. D. Hillier, J. Phys.: Condens. Matter **32**, 085601 (2020).

[62] G. M. Luke, A. Keren, L. P. Le, W. D. Wu, Y. J. Uemura, D. A. Bonn, L. Taillefer, and J. D. Garrett, Phys. Rev. Lett. **71**, 1466 (1993).

[63] J. Zhang, Z. Ding, C. Tan, K. Huang, O. O. Bernal, P.-C. Ho, G. D. Morris, A. D. Hillier, P. K. Biswas, S. P. Cottrell, H. Xiang, X. Yao, D. E. MacLaughlin, and L. Shu, Sci. Adv. **4**, eaao5235 (2018).

[64] A. J. Drew, F. L. Pratt, T. Lancaster, S. J. Blundell, P. J. Baker, R. H. Liu, G. Wu, X. H. Chen, I. Watanabe, V. K. Malik, A. Dubroka, K. W. Kim, M. Rössle, and C. Bernhard, Phys. Rev. Lett. **101**, 097010 (2008).

[65] J. A. T. Barker, R. P. Singh, A. D. Hillier, and D. M. Paul, Phys. Rev. B **97**, 094506 (2018).